Electronic Supplementary Material (ESI) for Journal of Materials Chemistry A.
This journal is © The Royal Society of Chemistry 2016.

Electronic Supporting Information

Bio-directed Morphology Engineering Towards Hierarchical 1D to 3D Macro/meso/nanoscopic *Morph*-tunable Carbon Nitride Assemblies for Enhanced Artificial Photosynthesis

Jun Xu,[ab] Han Zhou,*[ab] Kaiyu Shi,[a] Runyu Yan,[a] Yiwen Tang,[a] Jian Liu,[e] Jinhua Ye, [cd] Di Zhang[a] and Tongxiang Fan*[a]

[a] *State Key Lab of Metal Matrix Composites, Shanghai Jiaotong University, Shanghai 200240, China.*

E-mail addresses: hanzhou_81@sjtu.edu.cn; txfan@sjtu.edu.cn;

Fax: +86-21-34202749; Tel: +86-21-54747779

[b] *Advanced Energy Material and Technology Center, Shanghai Jiaotong University, Shanghai 200240, China.*

[c] *International Center for Materials Nanoarchitectonics (MANA), National Institute for Materials Science (NIMS), 1-1 Namiki, Tsukuba, Ibaraki 305-0044, Japan.*

[d] *TU-NIMS Joint Research Center, School of Materials Science and Engineering, Tianjin University, 92 Weijin Road, Nankai District, Tianjin 300072, China.*

[e] *Department of Chemistry, Northwestern University, Evanston, 60208, USA.*

Supplementary figures and tables

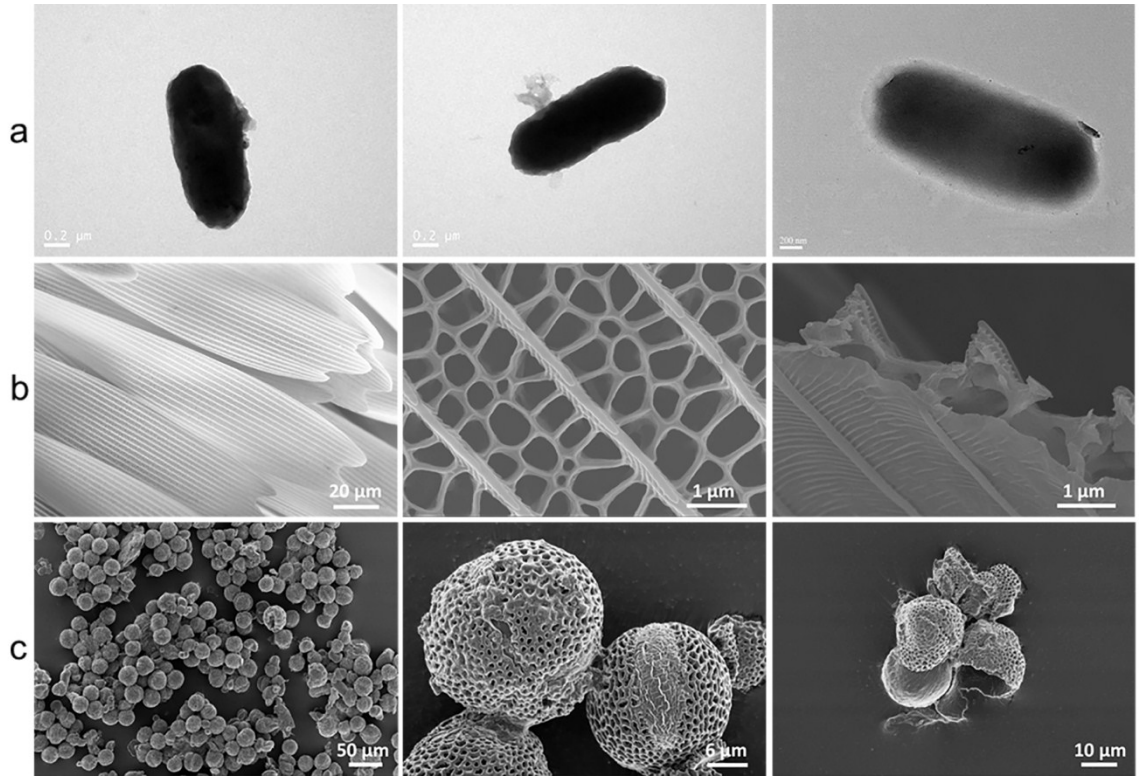

Figure S1. (a) TEM images of *Escherichia coli*, scale bar is 0.2 μm. (b) And (c) SEM images of *Papilio nephelus* butterfly wings and wall-broken cole pollen, respectively.

The rod-like *Escherichia coli* was selected as 1D architectures model. The diameter of the bacteria used here is approximately 0.80 μm. As for the 2D planar prototype, the back scales of original *Papilio nephelus* butterfly wings contain complex network structure, which consists of periodic inverse V-type ridges parallel to the longitudinal axis of the scale, a set of triple-row patterned hole arrays in the host lamina, an air space with disordered columnar pillars as upholders and a basal substrate. And the size of the triple-row patterned holes is about 0.7 μm. Here butterfly wing serves as 2D planar prototype because of its film feature though its elaborated structures are more complex than traditional 2D concept. The micro-spherical wall-broken cole pollen has a 3D core-shell structure and the hierarchical scaffolds of the shell are actually composed of well-

organized perpendicular columellae sandwiched between the reticular tectums and intimal lamina basalis. Holes in the 3D opening hierarchical porous networks possess a size of about 1 μm and the wall thickness is about 0.6 μm.

Table S1. BET surface area, BJH pore size and pore volume of the bio-directed SiO_2 and g-C_3N_4 samples.

Number	Samples	CTAB	BET Surface Area [m^2 g^{-1}]	BJH Pore Size [nm]	Pore Volume [cm^3 g^{-1}]
1	Butterfly wing-directed SiO_2	With	667.33	1.58	0.329
2	Cole pollen-directed SiO_2	With	734.63	1.65	0.380
3	Bulk g-C_3N_4	—	12.65	17.58	0.093
4	Butterfly wing-directed g-C_3N_4	With	59.40	13.14	0.171
5	Cole pollen-directed g-C_3N_4	with	71.09	12.82	0.162
6	*Butterfly wing-directed SiO_2*	*no*	*15.74*	—	—
7	*Cole pollen-directed SiO_2*	*no*	*41.83*	—	—
8	*Butterfly wing-directed g-C_3N_4*	*no*	*15.22*	—	—
9	*Cole pollen-directed g-C_3N_4*	*no*	*19.21*	—	—

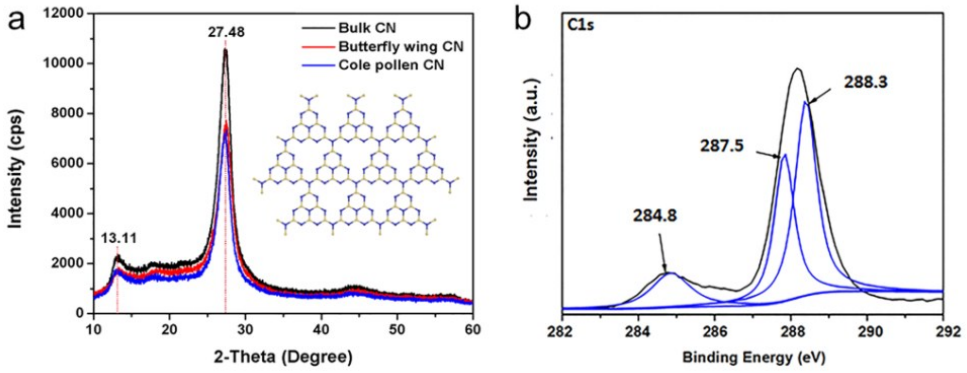

Figure S2. (a) X-ray diffraction (XRD) patterns of the bulk g-C_3N_4 and bio-directed g-C_3N_4. (b) XPS spectra of C 1s for the butterfly wing-directed g-C_3N_4.

The characteristic structural features of the g-C_3N_4 samples were verified by XRD. As we can see in Figure S2a, the XRD patterns for g-C_3N_4 samples are almost the same except the diffraction

intensity, revealing a quasi-graphitic structure with a planar stack of conjugated aromatic system, which is similar to the XRD patterns of g-C_3N_4 in the previous works. The most intense diffraction peak at 27.48° can be indexed as the (002) plane, corresponding to the characteristic interlayer stacking structure of aromatic systems, revealing an interlayer spacing of about 0.324 nm. While the weak diffraction peak at 13.11° relating to the (100) plane indicates the inplanar repeated tri-s-triazine units, such as the distance between the N holes in the crystal, corresponding to an interplanar spacing of 0.674 nm. The diffraction intensity of bio-directed g-C_3N_4 is weaker than the bulk g-C_3N_4, which is attributed to the differences in crystallinity.

Table S2. Elemental analysis of the obtained g-C_3N_4 samples.

Samples	N [wt%]	C [wt%]	H [wt%]	C/N atomic ratio
Bulk g-C_3N_4	60.165	34.125	1.8665	0.66
Bio-directed g-C_3N_4	53.525	29.715	2.4415	0.65

The g-C_3N_4 was synthesized with cyanamide as precursor through a complex thermal polymerization reaction at 550℃ under continuous Ar flowing. The product with C/N atomic ratio close to 0.65 could be identified as nitrogen-rich g-C_3N_4, which is concerned with precursor species and reaction conditions. Exclusion of adsorbed moisture, there are still tiny H existed, which was supposed to originate in uncondensed amino functions.

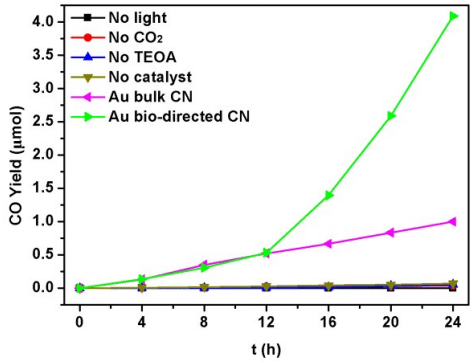

Figure S3. Typical time course of photocatalytic CO for 1 wt% Au loaded g-C_3N_4 in 20 vol% TEOA aqueous solution under visible light irradiation (λ > 400 nm).

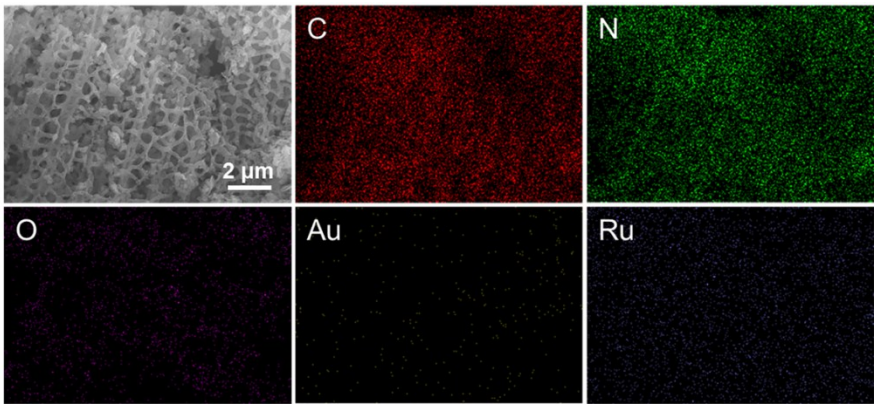

Figure S4. EDS mapping results of the Au and RuO_2 loaded bio-directed g-C_3N_4. After Au and RuO_2 were loaded, the biomorphic architecture of the bio-directed g-C_3N_4 has been definitely preserved with only a small degree of damage.

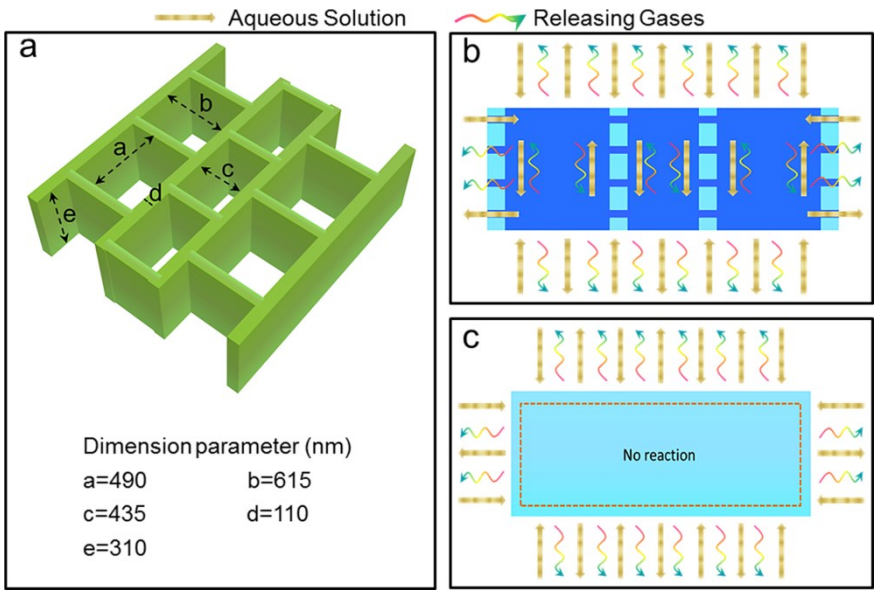

Figure S5. (a) Schematic diagram of the simplified butterfly wing-directed model and dimension parameter after converting to g-C_3N_4. Schematic diagram of the reaction interface for bio-directed model (b) and non-structural model (c). CO_2 gas is dissolved in aqueous solution. Releasing gases include CO and CH_4.

Dimension parameters of butterfly wing-directed model after converting to g-C_3N_4 are given in Figure S5a and the parameters of the non-structural model are set up accordingly. In the bio-directed model, aqueous solution can circulate in the hierarchical macro/meso/nanoscopic holes, where the catalytic reaction takes place (Figure S5b). And flow in macropores is predominant because of the amount of mesoporous is relatively small (Table S1). Nevertheless, only the surface area involves in the reaction in the non-structural model (Figure S5c). There is only trace of mesoporous existed in the non-structural model.

The flow in the structure is modeled with the Laminar Flow interface that solves the Navier-Stokes equations at steady state:[1]

$$\rho(u \cdot \nabla)u = \nabla \cdot \left[-pI + \mu\left(\nabla u + (\nabla u)^T\right) - \frac{2}{3}\mu(\nabla u)I \right] + F$$

$$\nabla \cdot (\rho u) = 0 \qquad \textbf{(1)}$$

Here, μ denotes the dynamic viscosity, *Ns* m^{-2}; u is the velocity, m s^{-1}; ρ is the density of the fluid, kg m^3; p is the pressure, Pa; and F is the volume force, N m^{-3}. A pressure difference drives the flow through the structure, as indicated by the boundary conditions:

$$p = p_{inlet} \qquad \text{inlet}$$

$$p = 0 \qquad \text{outlet}$$

At the wall the velocity is zero:

$$u = 0 \qquad \text{walls}$$

The catalytic reaction occurred in the APS was assumed to be a surface reaction (Figure S5b and S5c) and the chemical equation was basically defined as:

$$AS(s) + CO_2 \overset{hv}{\Rightarrow} CO + CH_4$$

Here *AS(s)* denotes the active substance involved in the reaction on the catalyst surface.

The reaction rate are:[2]

$$r_j = k_j^f \prod_{i=1}^{Q_r} c_i^{-v_{ij}} - k_j^r \prod_{i=1}^{Q_p} c_i^{v_{ij}} \qquad (2)$$

where the rate constants are given by the Arrhenius expression:

$$k_j = A_j exp\left(-\frac{E_j}{R_g T}\right) \qquad \textbf{(3)}$$

In equation 2, A_j is the frequency factor, and E_j is the activation energy, J mol^{-1}. Here temperature T is 293.15 K. The positive reaction rate constant k^f is set to be 4.5 m^3 s^{-1} mol^{-1} approximatively and the whole reaction is considered irreversible (i.e. k^r was zero). Thus the reaction rates can be written as follows:

$$r = k^f \cdot c_{AS} \cdot c_{CO_2} \quad \textbf{(4)}$$

The positive reaction rate constant k^f and surface species concentration c_{AS} are the same with no change for the two models in the whole process.

The mass balances are set up with the Transport of Diluted Species interface and solves the diffusion-convection equations at steady state:[3]

$$\frac{\partial c_i}{\partial t} + \nabla \cdot \left(- D_i \nabla c_i \right) + u \cdot \nabla c_i = R_i$$

$$N_i = - D_i \nabla c_i + u c_i \quad \textbf{(5)}$$

Here D_i denotes the diffusion coefficient, m^2 s^{-1}; c_i is the species concentration, mol m^{-3}; u equals the velocity, m s^{-1}; R_i represents the reaction term, mol m^{-3} s^{-1}; and N_i represents the boundary flux, mol m^{-2} s^{-1}.

No reactions take place in the fluid bulk. Rather, the reactions take place on the catalytic surfaces.

Table S3. Basic data used in the simulation.

Basic parameter	Value
Reactor volume	1 m^3
Reactor area	1 m^2
Initial CO_2 concentration	5 mol m^{-3}
Surface species concentration (c_{AS})	1 mol m^{-2}
External liquid flow velocity (u)	0.5 m s^{-1}
Frequency factor (A)	10^{-3} m^3 s^{-1} mol^{-1}
Activation energy (E)	3×10^4 J mol^{-1}
Ratio constant (R_g)	8.314 J mol^{-1} K^{-1}
Reaction temperature (T)	293.15 K
Reference pressure (p)	1 atm
Reaction rate constant (k)	4.5×10^{-9} m^3 s^{-1} mol^{-1}
Surface diffusivity (D)	5.4×10^{-6} cm^2 s^{-1}
Volume force (F)	0
Heat conductivity coefficient	0.02 W m^{-1} K^{-1}

Reaction rate constant was calculated according to Equation S3 mentioned above. The surface diffusivity was calculated according to Equation S15 in the following pages.

In order to investigate the influence of the hierarchical porous structures, gas diffusion mechanism is discussed to have a better understanding of micro-nano-scale effect on catalytic efficiency. Gas diffusion in porous media consists of several mechanisms: viscous flow, Knudsen diffusion, surface diffusion and molecular diffusion. Molecular diffusion is caused by collision between different component gas molecules. For a single gas species, collision between molecules results in viscous flow. Knudsen diffusion is generated from collision between molecules and the pore walls, while surface diffusion happens when adsorbed gas molecules creep along the pore surface.[3]

When the mean-free path of gas molecules is very small compared to the pore diameters, the

probability of collisions between molecules (Brownian motion) is much higher than collisions between molecules and pore walls; thus, single-component gas transport is mainly governed by viscous flow caused by the pressure gradient. Viscous flow can be modeled by Darcy's law:[4]

$$N_V = -\frac{\rho_m k_\infty}{\mu_m}(\nabla p_m) \quad \textbf{(6)}$$

Where N_V is the mass flux of viscous flow, kg m^{-2} s^{-1}; k_∞ is the intrinsic permeability of the porous media, m^2; p_m is the matrix gas pressure, Pa; ρ_m is the matrix gas density, kg m^{-3}; and μ_m is the matrix gas viscosity, Pa s.

Molecular diffusion refers to the relative motion of different gas species, and can be expressed as:[5]

$$N_A = -D_{AB}^{*}\rho_g(\nabla \omega_A) \quad \textbf{(7)}$$

Where N_A is the mass flux of component A of molecular diffusion, kg m^{-2} s^{-1}; D_{AB}^{*} is the effective molecular diffusivity of gases A and B, m^2 s^{-1}; ρ_g is the density of the mixture gas, kg m^{-3}; ω_A is the mass friction of component A.

When the pore space is so narrow that the mean-free path of gas molecules is very close to the pore diameter, collisions between molecules and pore walls dominate. Knudsen diffusion can be expressed as:[6]

$$N_K = -M_g D_K(\nabla C_m) \quad \textbf{(8)}$$

where N_K is the mass flux of Knudsen diffusion, kg m^{-2} s^{-1}; M_g is the molecular weight of gas, kg mol^{-1}; D_K is the Knudsen diffusivity, m^2 s^{-1}; C_m is the concentration of free gas in the porous

media, mol m^{-3}.

Surface diffusion only occurs in porous media where the gas is adsorbed onto the pore wall, and can be expressed as:[7]

$$N_S = - M_g D_S (\nabla C_s) \quad \textbf{(9)}$$

where N_S is the mass flux of surface diffusion, kg m^{-2} s^{-1}; D_S is the surface diffusivity, m^2 s^{-1}; C_S is the concentration of adsorbed gas, mol m^{-3}.

Gas diffusion mechanism in the matrix is determined by mutual effect of molecular diffusion, Knudsen diffusion and adsorption layer surface diffusion.

For accurate calculations, the Chapman-Enskog Formula has been found suitable for evaluating the molecular diffusivity at moderate temperatures and pressures. The equation is (for the binary gas mixture A, B) :[8,9]

$$D_{AB} = 0.0018583 * \frac{T^{3/2}\left(1/M_A + 1/M_B\right)^{1/2}}{p\sigma_{AB}^2 \Omega_{AB}} \quad \textbf{(10)}$$

Where D_{AB} = molecular diffusivity, cm^2 s^{-1}

T = temperature, K

M_A, M_B = molecular weights of gases A and B, g mol^{-1}

p = total pressure of the gas mixture, atm

σ_{AB}, ε_{AB} = constant in the Lennard-Jones potential-energy function for the molecular

pair AB; σ_{AB} is in Å

Ω_{AB} = collision integral, which would be unity if the molecules were rigid spheres and is a function of kT/ε_{AB} for real gases (k is Boltzmann constant, 1.3806505×10^{-23} J K^{-1})

$$\sigma_{AB} = \frac{1}{2}(\sigma_A + \sigma_B)$$

$$\varepsilon_{AB} = (\varepsilon_A \varepsilon_B)^{1/2}$$

For evaluating the Knudsen diffusivity we may use the following equation

$$(D_K)_A = 9.70 \times 10^3 * r\left(\frac{T}{M_A}\right)^{1/2} \quad \textbf{(11)}$$

Where $(D_K)_A$ = Knudsen diffusivity, cm^2 s^{-1}

r = pore radius, cm

The combined diffusivity D is given by (in the absence of surface diffusion):

$$D = \frac{1}{(1 - \alpha y_A)/D_{AB} + 1/(D_K)_A} \quad \textbf{(12)}$$

Where D = combined diffusivity with molecular diffusion and Knudsen diffusion, cm^2 s^{-1}

y_A = the mole fraction of A

α is related to the ratio of the diffusion rates of A and B by: $\alpha = 1 + \frac{N_B}{N_A}$

The effective diffusivity is:

$$D_e = \frac{\varepsilon}{\delta} D \quad \textbf{(13)}$$

Where D_e = effective diffusivity, $cm^2\ s^{-1}$

ε = the porosity

δ = the tortuosity factor which varies from less than unity to more than 6

The surface diffusivity is described by an Arrhenius-type expression:

$$D_s = k_A^{'} A_s \, exp\left(- \frac{E_s}{R_g T} \right) \quad \textbf{(14)}$$

Where D_s = surface diffusivity, $cm^2\ s^{-1}$

$k_A^{'}$= the linear form of the equilibrium constant

E_s = the activation energy for surface diffusion.

Such D_s values range from 10^{-3} to 10^{-6}, depending on the nature of the adsorbent and the amount adsorbed. The surface diffusivity of the reacting species in the simulation is assumed to depend on the temperature according to:[2,10]

$$D_s = 5 * 10^{-3} \cdot exp\left(- \frac{2000}{T} \right) \quad \textbf{(15)}$$

In this example, the temperature and pressure conditions are: T = 293.15 K, p = 1.0 atm.

The values of σ of the components are listed as follows:[8,9,11]

Table S4. Data required for the calculation of diffusivity.

Number	Gas species	Molecular weight M [g mol^{-1}]	σ [Å]	ε/k [K]
A	CO_2	44.01	3.941	195.2
B	CO	28.01	3.690	91.7
C	H_2O	18.015	2.641	809.1

So

$$\sigma_{AB}=3.816\ \text{Å},\ \sigma_{AC}=3.291\ \text{Å},\ \sigma_{BC}=3.166\ \text{Å}$$

$$\varepsilon_{AB}/k=133.79\ \text{K},\ \frac{kT}{\varepsilon_{AB}}=2.191,\ \Omega_{AB}=1.046$$

$$\varepsilon_{AC}/k=397.41\ \text{K},\ \frac{kT}{\varepsilon_{AC}}=0.738,\ \Omega_{AC}=1.682$$

$$\varepsilon_{BC}/k=272.39\ \text{K},\ \frac{kT}{\varepsilon_{BC}}=1.076,\ \Omega_{BC}=1.390$$

For the butterfly wing-directed model, Knudsen diffusion is predominant in the mesopores while molecular diffusion occupies a leading position in the macropores.

$$D_{AB}=0.0018583*\frac{293.15^{3/2}*(1/44.01+1/28.01)^{1/2}}{1.0*3.816^2*1.046}=0.148\ \text{cm}^2\ \text{s}^{-1}$$

$$D_{AC}=0.0018583*\frac{293.15^{3/2}*(1/44.01+1/18.015)^{1/2}}{1.0*3.291^2*1.682}=0.143\ \text{cm}^2\ \text{s}^{-1}$$

$$D_{BC}=0.0018583*\frac{293.15^{3/2}*(1/28.01+1/18.015)^{1/2}}{1.0*3.166^2*1.390}=0.202\ \text{cm}^2\ \text{s}^{-1}$$

r =13.14 nm, $(D_K)_A=9.70\times10^3*(13.14*10^{-7})*\left(\frac{293.15}{44.01}\right)^{1/2}=0.033\ \text{cm}^2\ \text{s}^{-1}$

$$(D_K)_B=9.70\times10^3*(13.14*10^{-7})*\left(\frac{293.15}{28.01}\right)^{1/2}=0.041\ \text{cm}^2\ \text{s}^{-1}$$

For the non-structural model, the molecular diffusivity can be ignored.

r =17.58 nm, $(D_K)_A' = 9.70 \times 10^3 * (17.58 * 10^{-7}) * \left(\frac{293.15}{44.01}\right)^{1/2} =$ 0.044 $cm^2\ s^{-1}$

$$(D_K)_B' = 9.70 \times 10^3 * (17.58 * 10^{-7}) * \left(\frac{293.15}{28.01}\right)^{1/2} =$$ 0.055 $cm^2\ s^{-1}$

From Table S1 we can infer that the porosity of butterfly wing-directed g-C_3N_4 is much higher than the bulk g-C_3N_4, so the effective diffusivity of butterfly wing-directed model will be larger too.

The surface diffusivity of the two models is the same according to:

$$D_s = D_S^{'} = 5 * 10^{-3} \cdot exp\left(-\frac{2000}{293.15}\right) = 5.445 \times 10^{-6}\ cm^2\ s^{-1}$$

The calculation results are listed as follows.

Table S5. Calculation results of diffusivity for CO_2 and CO transport.

Model class	Molecular diffusivity [$cm^2\ s^{-1}$]			Knudsen diffusivity [$cm^2\ s^{-1}$]		Surface diffusivity [$cm^2\ s^{-1}$]
	CO_2-CO	CO_2-H_2O	CO-H_2O	CO_2	CO	
Butterfly wing-directed model	0.148	0.143	0.202	0.033	0.041	5.445×10^{-6}
Non-structural model	—	—	—	0.044	0.055	5.445×10^{-6}

References

1 M. Fadaei and R. Mohammadi, *Energy Convers. Manage.*, 2015, **106**, 93-100.

2 http://cn.comsol.com/model/download/269841/models.chem.tortuous_reactor.pdf.

3 W. Wang, J. Yao, H. Sun and W.-H. Song, *Pet. Sci.* , 2015, **12**, 664-673.

4 W. Kast and C.-R. Hohenthanner, *Int. J. Heat Mass Transfer*, 2000, **43**, 807-823.

5 E. L. Cussler, *Diffusion: mass transfer in fluid systems*, Cambridge university press, 2009.

6 F. A. Florence, J. Rushing, K. E. Newsham and T. A. Blasingame, in *Rocky mountain oil & gas technology symposium*, Society of Petroleum Engineers, 2007.

7 X. Xiong, D. Devegowda, M. Villazon, G. German, R. F. Sigal and F. Civan, in *SPE annual technical conference and exhibition*, Society of Petroleum Engineers, 2012.

8 J. M. Smith, *Chemical engineering kinetics*, 1981.

9 P. Chinda, S. Chanchaona, P. Brault and W. Wechsatol, *J. Sus. Energy Environ.*, 2010, **1**, 185-196.

10 P. Schneider and J. M. Smith, *AlChE J.*, 1968, **14**, 762-771.

11 B. Todd and J. B. Young, *J. Power Sources*, 2002, **110**, 186-200.